Available online at www.sciencedirect.com
SCIENCE DIRECT
Journal of Sound and Vibration 293 (2006) 878–887
JOURNAL OF SOUND AND VIBRATION
www.elsevier.com/locate/jsvi

Analytical and experimental study of sleeper SAT S 312 in slab track Sateba system

C. Guigou-Carter[a,*], M. Villot[a], B. Guillerme[b], C. Petit[c]

[a]CSTB, 24 Rue Joseph Fourier, 38400 St Martin d'Hères, France
[b]Sateba, Rue J.L. Thénard, Z.I. Chalon/Saône, 71100 Chalon/Saône, France
[c]Sateba, Tour Ariane, 5 Place de la pyramide, 75088 Paris La Défense Cedex, France

Accepted 26 August 2005
Available online 3 February 2006

Abstract

In this paper, a simple prediction tool based on a two-dimensional model is developed for a slab track system composed of two rails with rail pads, sleepers with sleeper pads, and a concrete base slab. The track and the slab are considered as infinite beams with bending stiffness, loss factor and mass per unit length. The track system is represented by its impedance per unit length of track and the ground by its line input impedance calculated using a two-dimensional elastic half-space ground model based on the wave approach. Damping of each track component is modelled as hysteretic damping and is taken into account by using a complex stiffness. The unsprung mass of the vehicle is considered as a concentrated mass at the excitation point on the rail head. The effect of the dynamic stiffness of the sleeper pads on the vibration isolation is studied in detail, the vibration isolation provided by the track system being quantified by an insertion gain in dB per one-third octave band. The second part of this paper presents an experimental test rig used to measure the dynamic stiffness of the sleeper pads on a full width section of the track (two rails). The experimental set-up is submitted to vertical as well as horizontal static loads (via hydraulic jacks) and an electrodynamic shaker is used for dynamic excitation of the system. The determination of the dynamic stiffness of the sleeper pads is based on the approach called the "direct method". The limitations of the experimental set-up are discussed. The measurement results for one type of sleeper pad are presented.

1. Introduction

Nowadays, new railway tracks are installed close to existing buildings in cities. Track-work has to be designed to reduce the transmission of vibration caused by the running of the trains on metal rails, the rail joints, and rail defects, to the neighbouring buildings. This vibration, as well as the corresponding re-radiated noise, are perceptible and therefore may cause great annoyance to residents. Ground vibration propagation from railways has been investigated previously using two- and three-dimensional models [1–3].

*Corresponding author. Tel.: +33 476762525; fax: +33 476442046.
E-mail addresses: cguigou@cstb.fr (C. Guigou-Carter), villot@cstb.fr (M. Villot), b.guillerme@sateba.com (B. Guillerme), c.petit@sateba.com (C. Petit).

0022-460X/$ - see front matter © 2006 Elsevier Ltd. All rights reserved.
doi:10.1016/j.jsv.2005.08.053

In this paper, a simple prediction tool based on a two-dimensional model is first developed (Section 2) for a slab track system composed of two rails with rail pads, sleepers with sleeper pads, and a concrete base slab. The track and the slab are considered as infinite beams with bending stiffness, loss factor and mass per unit length. The track system is represented by its impedance per unit length of track and the ground by its line input impedance calculated using a two-dimensional elastic half-space ground model based on the wave approach. Damping of each track component is modelled as hysteretic damping (as opposed to viscous damping) and is taken into account by using a complex stiffness. The unsprung mass of the vehicle is considered as a concentrated mass at the excitation point on the rail head. The effect of the sleeper pad's dynamic stiffness on the vibration isolation is studied in detail. The vibration isolation provided by the track system is quantified by an insertion gain in dB per one-third octave band. The second part of this paper (Section 3) presents an experimental rig, set up in the Sateba laboratory at the Chalon/Saône production site, to measure the dynamic stiffness of the sleeper pads on a full width section of the track (two rails). The experimental set-up is submitted to vertical as well as horizontal static loads (via hydraulic jacks) and an electro-dynamic shaker is used for a dynamic excitation of the system. The determination of the dynamic stiffness of the sleeper pads is based on the approach called the "direct method" derived from the European standard EN ISO 10846-2 [4]. The limitations of the experimental set-up are discussed. The measurement results for one type of sleeper pad are presented.

2. Track system prediction model

2.1. Model description

The model developed is two dimensional and is represented diagrammatically in Fig. 1. The track (two rails) and the concrete base slab are considered as infinite beams and are characterized by their mass per unit length (m_{rail} and m_{slab}, respectively) and their complex bending stiffness taking into account the damping (B_{rail} and B_{slab}, respectively). It should be noted that damping for each track component is modelled as hysteretic and is therefore taken into account by using a complex stiffness. In the track system proposed, sleeper pads are inserted between sleepers and concrete slab and the rail pads are located between rail and sleepers. The rail and sleeper pads are defined by their dynamic stiffness per unit length denoted K_{pad} and K_{slp}, respectively. The sleepers considered are twin-block sleepers and are represented by their mass per unit length m_{slp}. The ground is modelled as a semi-infinite two-dimensional system defined by its line input impedance Z_{ground} calculated using a two-dimensional elastic half-space ground model based on the wave approach [5]. The unsprung mass of the vehicle denoted M_u is considered as a concentrated mass at the excitation point on the rail head. Both the unsprung mass and the excitation force are applied on the rail at the position $x = 0$. The displacement of the rails, the sleepers and the concrete base slab are denoted w_{rail}, w_{slp} and w_{slab}, respectively. The time dependence has the form $e^{j\omega t}$ (where ω is the angular frequency) and will be omitted in the following for brevity.

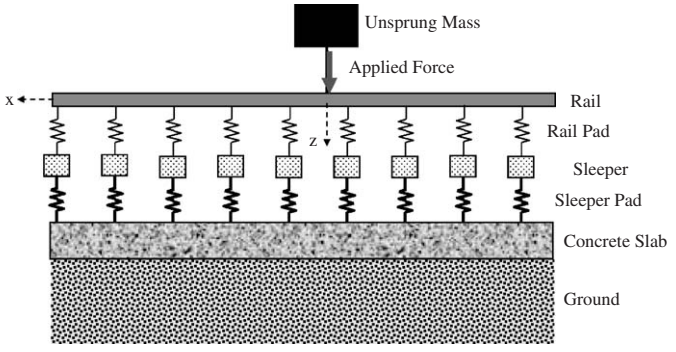

Fig. 1. Diagrammatic representation of the model.

The forces applied to the rail and the slab by the system composed of the rail pads, the sleepers and the sleeper pads, are given by

$$F_{\text{rail}}(x) = -K_{\text{pad}}(w_{\text{rail}}(x) - w_{\text{slp}}(x)),$$
$$F_{\text{slab}}(x) = K_{\text{slp}}(w_{\text{slp}}(x) - w_{\text{slab}}(x)). \tag{1}$$

The displacement of the sleeper mass is then given by the following equation of motion:

$$-m_{\text{slp}}\omega^2 w_{\text{slp}}(x) = K_{\text{pad}}(w_{\text{rail}}(x) - w_{\text{slp}}(x)) - K_{\text{slp}}(w_{\text{slp}}(x) - w_{\text{slab}}(x)). \tag{2}$$

Replacing the sleeper mass displacement in the expression of the forces applied to the rail and the slab, i.e. Eq. (1), yields

$$F_{\text{rail}}(x) = -K_{\text{pad}}\left(\left[1 - \frac{K_{\text{pad}}}{[K_{\text{pad}} + K_{\text{slp}} - m_{\text{slp}}\omega^2]}\right] w_{\text{rail}}(x) - \frac{K_{\text{slp}}}{[K_{\text{pad}} + K_{\text{slp}} - m_{\text{slp}}\omega^2]} w_{\text{slab}}(x)\right),$$
$$F_{\text{slab}}(x) = K_{\text{slp}}\left(\frac{K_{\text{pad}}}{[K_{\text{pad}} + K_{\text{slp}} - m_{\text{slp}}\omega^2]} w_{\text{rail}}(x) - \left[1 - \frac{K_{\text{slp}}}{[K_{\text{pad}} + K_{\text{slp}} - m_{\text{slp}}\omega^2]}\right] w_{\text{slab}}(x)\right). \tag{3}$$

The equation of motion of the coupled system in the spatial domain is then given by

$$(B_{\text{rail}}\nabla^4 - \omega^2 m_{\text{rail}}) w_{\text{rail}}(x) = F_{\text{rail}}(x) + (F + \omega^2 M_u w_{\text{rail}}(0))\delta(x - 0),$$
$$(B_{\text{slab}}\nabla^4 - \omega^2 m_{\text{slab}}) w_{\text{slab}}(x) = F_{\text{slab}}(x) - \mathrm{j}\omega Z_{\text{ground}}(x) w_{\text{slab}}(x). \tag{4}$$

Taking the Fourier transform ($x \to k_x$), Eq. (4) yields

$$\left\{(B_{\text{rail}}k_x^4 - \omega^2 m_{\text{rail}}) + K_{\text{pad}} - \frac{(K_{\text{pad}})^2}{K_{\text{pad}} + K_{\text{slp}} - \omega^2 m_{\text{slp}}} - A_{\text{slab}\to\text{rail}}(k_x)\left[\frac{K_{\text{pad}}K_{\text{slp}}}{K_{\text{pad}} + K_{\text{slp}} - \omega^2 m_{\text{slp}}}\right]\right\}\tilde{w}_{\text{rail}}(k_x) = \bar{F},$$
$$\tilde{w}_{\text{slab}}(k_x) = A_{\text{slab}\to\text{rail}}(k_x)\tilde{w}_{\text{rail}}(k_x), \tag{5}$$

where the following notations are used:

$$\bar{F} = F + \omega^2 M_u w_{\text{rail}}(0),$$
$$A_{\text{slab}\to\text{rail}}(k_x) = \frac{\left[\dfrac{K_{\text{pad}}K_{\text{slp}}}{K_{\text{pad}} + K_{\text{slp}} - \omega^2 m_{\text{slp}}}\right]}{\left[(B_{\text{slab}}k_x^4 - \omega^2 m_{\text{slab}}) + K_{\text{slp}} - \dfrac{(K_{\text{slp}})^2}{K_{\text{pad}} + K_{\text{slp}} - \omega^2 m_{\text{slp}}} + \mathrm{j}\omega Z_{\text{ground}}(k_x)\right]}. \tag{6}$$

Taking the inverse Fourier transform, the rail and the slab displacements at the position $x = 0$ can be deduced from

$$w_{\text{rail}}(0) = \bar{F}\,\bar{Y}_{\text{rail}} = (F + \omega^2 M_u w_{\text{rail}}(0))\,\bar{Y}_{\text{rail}},$$
$$w_{\text{slab}}(0) = \bar{F}\,\bar{Y}_{\text{slab}} = (F + \omega^2 M_u w_{\text{rail}}(0))\,\bar{Y}_{\text{slab}}, \tag{7}$$

with

$$\bar{Y}_{\text{rail}} = \frac{1}{2\pi}\int_{-\infty}^{+\infty} \frac{\mathrm{d}k_x}{\left((B_{\text{rail}}k_x^4 - \omega^2 m_{\text{rail}}) + K_{\text{pad}} - \dfrac{K_{\text{pad}}^2 + A_{\text{slab}\to\text{rail}}(k_x)K_{\text{pad}}K_{\text{slp}}}{K_{\text{pad}} + K_{\text{slp}} - \omega^2 m_{\text{slp}}}\right)},$$
$$\bar{Y}_{\text{slab}} = \frac{1}{2\pi}\int_{-\infty}^{+\infty} \frac{A_{\text{slab}\to\text{rail}}(k_x)\mathrm{d}k_x}{\left((B_{\text{rail}}k_x^4 - \omega^2 m_{\text{rail}}) + K_{\text{pad}} - \dfrac{K_{\text{pad}}^2 + A_{\text{slab}\to\text{rail}}(k_x)K_{\text{pad}}K_{\text{slp}}}{K_{\text{pad}} + K_{\text{slp}} - \omega^2 m_{\text{slp}}}\right)}. \tag{8}$$

Eq. (7) yields the rail and slab displacements at the position $x = 0$:

$$w_{\text{rail}}(0) = \frac{F\,\bar{Y}_{\text{rail}}}{1 - \omega^2 M_u \bar{Y}_{\text{rail}}},$$
$$w_{\text{slab}}(0) = \frac{F\,\bar{Y}_{\text{slab}}}{1 - \omega^2 M_u \bar{Y}_{\text{rail}}}. \tag{9}$$

The vibration isolation provided by the track system is quantified by an insertion gain in dB per one-third octave band, defined as the difference between the vertical vibration velocity level at the concrete slab/ground interface, predicted for the proposed track-work (i.e. with the sleepers and sleeper pads) and a reference track that does not include either the sleepers or sleeper pads (only the rail pads are included between the rail and the concrete slab). Therefore, a positive insertion gain corresponds to vibration amplification, while a negative one yields a vibration decrease.

2.2. Model results

Insertion gains are then calculated with sleeper pads having different dynamic stiffness per unit length K_{slp}; in the calculation, the pad dynamic stiffness is assumed to be constant over the whole frequency range. The insertion gains are calculated for three types of trains: (1) the Eurostar with a maximum unsprung mass of 2150 kg/axle, (2) a domestic passenger stock with a maximum unsprung mass of 1309 kg/axle, and (3) a freight stock with a maximum unsprung mass of 3750 kg/axle.

The sleepers correspond to a mass per unit length of 350 kg/m (210 kg sleeper spaced by 0.6 m); the loss factor of the sleeper pads is taken to be 16% (representative of materials used for sleeper pads according to manufacturer's data sheet). The characteristics of the rail, the concrete slab and the ground are given in Table 1. The rail pads are assumed to have a dynamic stiffness per unit length K_{pad} of 720 MN/m^2 and a loss factor of 20%.

The insertion gain for the different trains is presented in Figs. 2–4 for the different sleeper pad dynamic stiffnesses considered, i.e. 35, 60 and 106 MN/m^2, respectively. As expected, the insertion gain presents a maximum, corresponding to a vibration increase of the concrete slab, at the resonance frequency of the system. This resonance frequency is modified by the sleeper pad stiffness as well as by the unsprung mass

Table 1
System components characteristics

Component	Mass per unit length (kg/m)	Bending stiffness (MNm^2)	Loss factor (%)	
Rail	120	12.65	0.1	
Slab	3668	1000	10.0	
	Density (kg/m^3)	Young's modulus (MN/m^2)	Loss factor (%)	Poisson ratio
Ground	2000	372	10.0	0.47

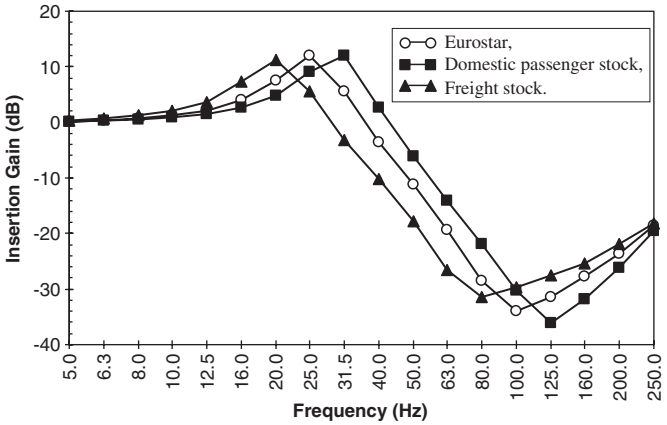

Fig. 2. Insertion gain for sleeper pads of dynamic stiffness 35 MN/m^2; ○—○ Eurostar, ■—■ domestic passenger stock, ▲—▲ Freight stock.

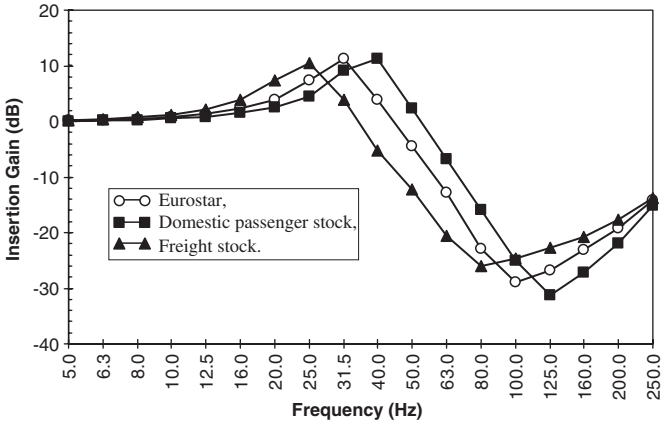

Fig. 3. Insertion gain for sleeper pads of dynamic stiffness 60 MN/m^2; ○—○ Eurostar, ■—■ domestic passenger stock, ▲—▲ Freight stock.

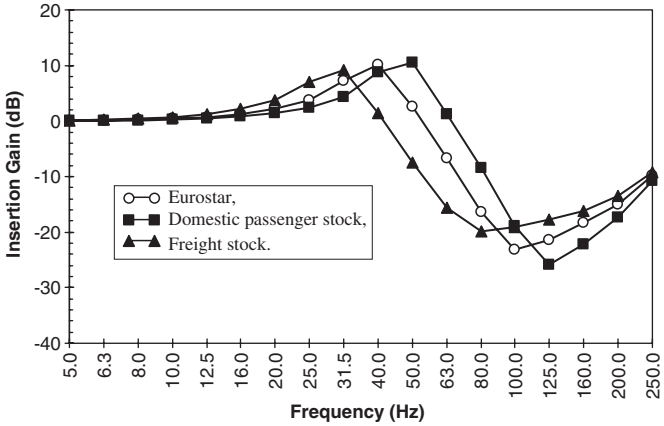

Fig. 4. Insertion gain for sleeper pads of dynamic stiffness 106 MN/m^2; ○—○ Eurostar, ■—■ domestic passenger stock, ▲—▲ Freight stock.

corresponding to the type of train considered. This resonance frequency decreases with a reduction of the sleeper pad dynamic stiffness. In the case of the Eurostar train, the resonance frequency changes from 31.5 to 25 Hz when the dynamic stiffness decreases from 60 to 35 MN/m^2. An increase of the unsprung mass (corresponding to the type of train) also yields a decrease of the resonance frequency. In the case of sleeper pads with 60 MN/m^2 in dynamic stiffness, the resonance frequency decreases from 40 Hz for the domestic passenger stock (corresponding the lightest unsprung mass considered) to 31.5 Hz for the Eurostar train, and to 25 Hz for the freight stock (the heaviest unsprung mass considered). A vibration decrease (negative insertion gain) is obtained above the resonance frequency. The maximum value of vibration decrease depends on the sleeper pad dynamic stiffness: the lowest sleeper pad dynamic stiffness is associated with the highest vibration decrease. In the case of the Eurostar train, the maximum vibration decrease occurs at 100 Hz and is 34 dB for the sleeper pads with dynamic stiffness of 35 MN/m^2 and 23 dB for those with dynamic stiffness of 106 MN/m^2.

This model provides a simple tool to choose sleeper pads with respect to their stiffness that respects specified mitigation levels.

3. Experimental test rig for sleeper pad stiffness measurements

The principal aim of the tests is to measure the dynamic characteristics of a prototype length of the slab track systems. The tests should be at conditions considered to be as representative as possible of in situ

operational conditions. Currently, no standard for the testing and reporting of the acoustic stiffness at the frequencies and load conditions associated with ground-borne noise generated by heavy rail is available. The dynamic stiffness measurement is performed for two different vertical static loads; for each vertical static load, the measurements were performed with and without a horizontal static load.

The experimental rig is set up in the Sateba laboratories located at Chalon/Saône (France). This laboratory has the 500 kN capacity test rig to be used for the vertical load/deflection tests. This static and quasi-static test rig was adapted to perform the dynamic tests in order to determine the dynamic stiffness of the sleeper pads.

3.1. Measurement principle

Fig. 5 presents a schematic view of the test rig for the dynamic test. The test rig for the dynamic test, as presented in Fig. 5, corresponds to that shown in the European standard NF EN ISO 10846-2 [4]. It allows the dynamic stiffness of the tested element to be determined using the approach called the "direct method". The blocking mass m_2 is an important component since it has to behave as a rigid element in the frequency range of interest in order to distribute the forces evenly. The excitation mass m_1 has to provide a uniform loading on the tested element; it has to be as small and light as possible and, at the same time, has to behave as a rigid element in the frequency range of interest. The displacement of both masses is then measured as well as the blocking forces. In this case, the dynamic stiffness of the tested element (transfer dynamic stiffness) is given by the expression

$$K2,1 \approx (F_{\text{blocking}}/u_1),$$

where F_{blocking} is the blocked force and u_1 is the displacement of the mass m_1.

The measurements are assumed to be valid if the displacement ratio between the two masses is larger than 15 dB. Note that in the standard in EN ISO 10846-2 [4], this requirement is 20 dB (i.e. stronger). When a lateral static load is applied to the test rig, this condition does not have to be verified.

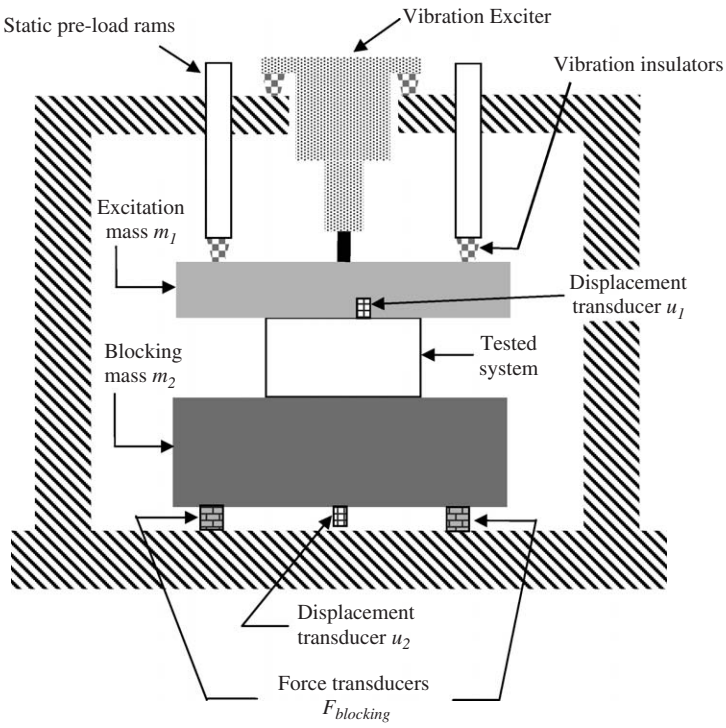

Fig. 5. Schematic view of the rig for "direct method" measurement.

Furthermore, the difference between the approximate blocking force $F_{\text{total blocking}}$ and the measured blocking force F_{blocking} is equal to the inertial force $F_{\text{inertial}} = m_2 (2\pi f)^2 u_2$. Therefore, the measured blocking force F_{blocking} can be corrected by the inertial force as follows:

$$F_{\text{total blocking}} = F_{\text{blocking}} + F_{\text{inertial}} = F_{\text{blocking}} + m_2(2\pi f)^2 u_2.$$

The measurements are assumed to be valid if the correction associated with the inertial force is lower than 0.8 dB, corresponding to an error on the blocking force due to the inertial force of 10%. Note that in the standard EN ISO 10846-2 [4], an error on the blocking force due to the inertial force of only 6% is allowed.

3.2. Test rig adaptation for dynamic measurements

The Sateba laboratory located at Chalon/Saône (France), has a 500 kN static load test rig. This test rig was adapted to perform the dynamic tests. A photograph of the test rig is presented in Fig. 6. The static load is applied to the track system through a U-shaped support and four vibration isolators. Each of these vibration isolators is composed of five layers of the softest resilient pad under test and each of these layers has a surface area of about a quarter of the resilient pad. The total stiffness of the four vibration isolators is then at least 10 times lower than that of the tested system. The dynamic excitation, through an electro-dynamic shaker, is applied directly to a figure-of-eight shaped support, corresponding to the excitation mass m_1. The excitation mass m_1 rests on the two rail heads that are 0.6 m in length; the rail profile is UIC 60. The blocking mass m_2, a concrete slab, was made out of reinforced concrete framed by steel beams with a mass of approximately 950 kg. Each sleeper block and its associated resilient pad are encased in a rigid plastic boot embedded in the

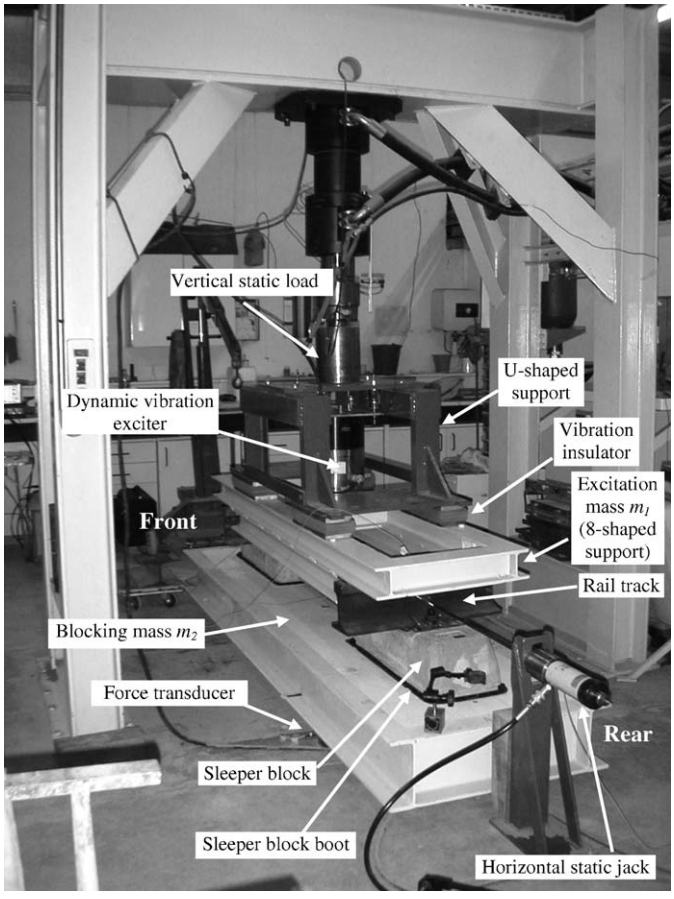

Fig. 6. General view of the test arrangement.

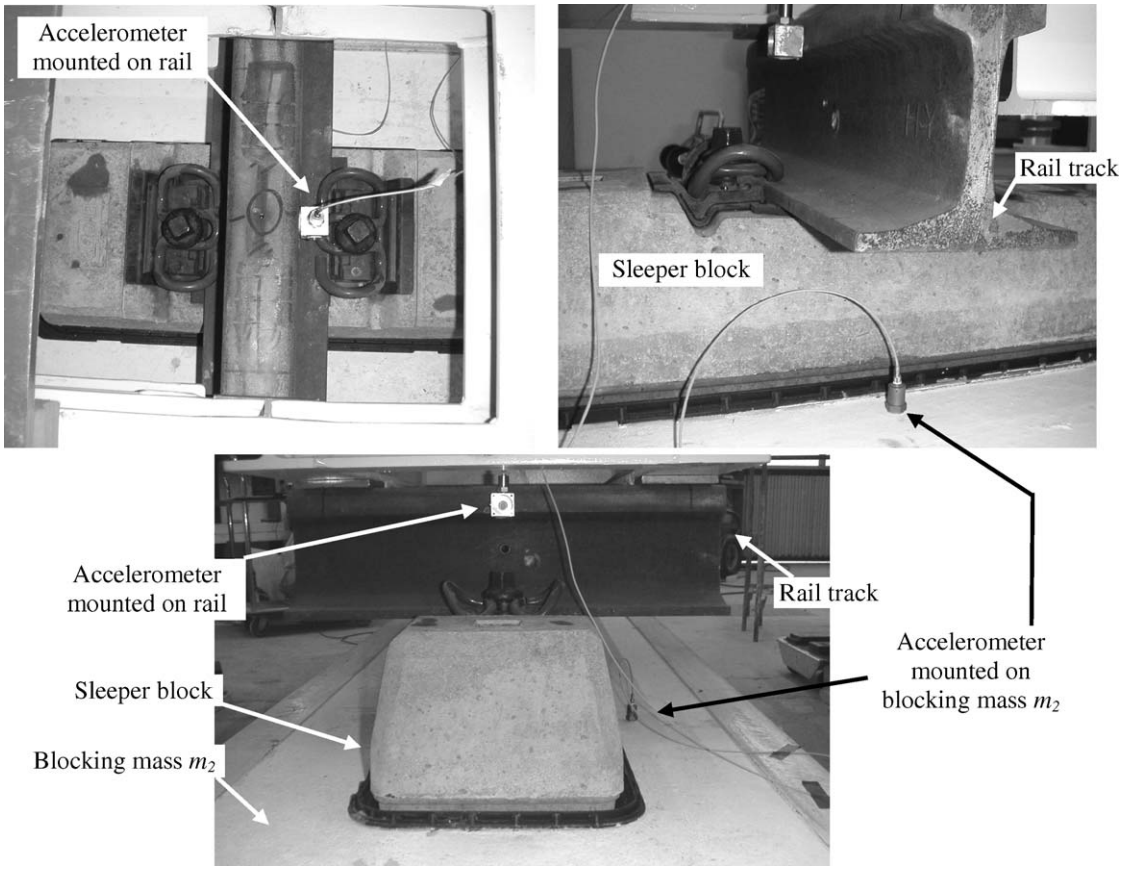

Fig. 7. Mounting of the accelerometers on test rig.

concrete slab. The boot for each sleeper block has some lateral pads to allow the vertical and horizontal motion of the sleeper block inside. The sleeper is fitted with a steel tie bar connecting the two blocks. Two rail pads are used between the rails and the sleeper; each rail is fixed to the sleeper by two clips maintained with two steel screws (see Fig. 7). Furthermore, the terms "front" and "rear" are used to differentiate the two rails and sleeper blocks, as shown in Fig. 6.

In order to improve the load distribution on the force transducers, only three force transducers, two in the rear and one in the front, were placed under the blocking mass m_2. They allowed the total blocking force to be measured.

The vibration exciter is suspended from the U-shaped support via four spring suspensions for decoupling: the resonance frequency for the total mass of the shaker and plate is intended to be around 3.5 Hz. The connection of the vibration exciter and the excitation mass m_1 (figure-of-eight shaped support) is achieved with a stinger screwed at both ends.

Four accelerometers were mounted on the test rig for measuring the vertical displacement: one on each rail head and one mounted on the blocking mass m_2 by the side of each sleeper block. Fig. 7 presents some views of the accelerometer mounting locations. It should be noted that since the accelerometers are located directly on the rail heads rather than on the excitation mass, the rigidity of this excitation mass m_1 is of relatively low importance (for a lower rigidity less dynamic force will be transmitted to the rails but the dynamic stiffness of the tested system that is obtained should remain unchanged). The difference in displacement between the two (front and rear) rail heads should not exceed 15%, implying that the excitation is relatively well centred on the tested system (vertical motion is then dominant and rotation effects are very limited). This limit is only valid when no lateral static load is applied to the test rig.

A lateral load has also to be applied on the rails of test rig to simulate the effect of the train going through a curve. The system used in this experiment can be seen in Fig. 6: a cylindrical rod fixed on both rails allows the lateral load to be applied on both rails. The two rails are pulled in the same direction.

The force distribution between the rear and the front of the experimental rig was verified with the three force transducers positioned under the blocking mass when different vertical static loads were applied with the hydraulic jack to the system. It was found to be good. The balance between the front and rear forces under dynamic excitation (via the shaker) was also found to be satisfactory.

The vibration levels on the floor of the laboratory were measured to verify that the vibration pollution associated with the vibration of the hydraulic jack support (directly connected to the ground around the test rig) was negligible. The static force was set to 40 kN. When no dynamic excitation is applied to the test rig, all the measured vibration levels are very low. When applying the dynamic excitation the vibration level of the rail is important at the excitation frequency; the vibration levels of the laboratory floor are increased but stay low compared to those of the rail and the blocking mass. Furthermore, the horizontal velocity of both rails and both sleeper blocks was measured and was found negligible compared with the associated vertical velocity.

The modal behaviour of the blocking mass m_2 was investigated. Several zones of resonance behaviour in the low frequency range were observed around 100 and 125 Hz as well as around 156 Hz. Therefore, the dynamic stiffness measurements were performed for the excitation frequencies 8, 16, 31.5 and 63 Hz; they will be invalid at the excitation frequency 125 Hz.

The dynamic stiffness is calculated based on the total blocking force (i.e. the blocking force measured by the three force transducers corrected by the inertial force) and either the vertical velocity measured on the front, or that measured on the rear rail; therefore two dynamic stiffness values, i.e. one for the rear sleeper pad and one for the front sleeper pad are obtained for the system. The dynamic stiffness presented below is then obtained as an average of the front and rear dynamic stiffness results.

3.3. Dynamic measurement results

The sleeper pad considered in this paper has a static stiffness of 13.5 MN/m and a quasi-static stiffness of 14.6 MN/m (provided by the manufacturer). It should correspond to a dynamic stiffness of 18 MN/m per rail seat (assuming a ratio of 1.25 between the dynamic and quasi-static stiffness). These resilient pads should then correspond to the sleeper pads with the dynamic stiffness per unit length of 60 MN/m^2 used for the predictions in Section 2 (two pads corresponding to 36 MN/m spaced by 0.6 m).

The measurement of the dynamic stiffness was performed for two different vertical static loads, corresponding to 40 kN and 64 kN, respectively. For a vertical static load of 40 kN, a horizontal static load of 10 kN was also considered; for the vertical static load of 64 kN, the associated horizontal static load was of 5 kN. It should be noted that the lateral load decreases with the increase of the vertical load since it is assumed that the heaviest trains (the largest vertical load) will have a reduced speed going through a curve and thus will correspond to a lower lateral load than a lighter train. By means of example, Table 2 presents the dynamic characterizations for this resilient pad for the different static loads (vertical and horizontal) considered; only results at the excitation frequency of 8 Hz are given for reasons of confidentiality.

First, it should be noticed that the dynamic load was well distributed between the two rails: the displacement difference is below the 15% allowed when no lateral static load is applied. The decoupling between the rail and the blocking mass vibration was found to be quite good, especially up to 31.5 Hz; it was very low at 125 Hz as expected since the blocking mass has resonance frequencies in that frequency range. The blocking force correction due to the inertial force (associated with the blocking mass) became quite significant (much larger than the requirements) at and above 63 Hz. Therefore, the measurement method and the test rig can only be validated for the determination of the dynamic stiffness of the resilient pads for excitation frequencies below 50 Hz. The measurements were performed at 8, 16 and 31.5 Hz.

The measured dynamic stiffness increases with the applied vertical load as well as with the applied horizontal load. It also increases with the excitation frequency (not shown). The measured dynamic stiffnesses are close to the expected value of 18 MN/m. The increase in dynamic stiffness associated with the lateral static load is less significant for the high vertical load of 64 kN than for the low vertical load of 40 kN. This increase of the measured dynamic stiffness when a lateral load is applied is associated with several factors: first, the

Table 2
Measurement results of the resilient pad dynamic stiffness at 8 Hz

Static load	Vertical 40 kN	Vertical 40 kN Horizontal 10 kN	Vertical 64 kN	Vertical 64 kN Horizontal 5 kN
Rear/front displacement difference (%)	5.8	10.4	1.9	12.0
Front decoupling (dB)	21.3	19.0	19.5	16.2
Rear decoupling (dB)	22.6	24.1	20.7	21.4
Blocking force F_{blocking} (N)	125.10	126.68	111.29	111.51
Total Blocking force $F_{\text{blocking total}}$ (N)	126.04	127.60	112.17	112.45
Blocking force error (%)	0.7	0.7	0.8	0.8
Pad dynamic stiffness (MN/m) With inertial force correction	12.9	14.4	15.2	16.9

sleeper pads are submitted to shearing then increasing the dynamic stiffness and second (and probably the more important effect) the sleepers come into contact with the lateral pads in the sleeper boot. For the excitation frequency of 8 Hz, the increase associated with the lateral load is around 12% for both vertical static loads. Furthermore, for the vertical static load of 40 kN, an increase in dynamic stiffness of more than 20% is obtained for the frequencies of 16 and 31.5 Hz, while for the vertical static load of 64 kN, an increase in dynamic stiffness of up to 20% is obtained.

4. Conclusions

In this paper, a simple two-dimensional model has been presented to predict the performance of a slab track system. The effect of the sleeper pad dynamic stiffness on the vibration isolation provided by the track system has been studied. This tool can be used to define sleeper pad dynamic stiffness corresponding to specific mitigation levels. In the second part of the paper, an experimental rig to measure the dynamic stiffness of the sleeper pads on a full width section of the track has been presented and its limitations have been discussed. This experimental rig allows vertical and horizontal static loads to be applied, as well as a dynamic load to the system. Example measurement results have been presented for some sleeper pads.

Acknowledgements

The work presented in this paper has been carried out for Sateba, a manufacturer of concrete sleepers, within the framework of the construction of the new Eurostar train track below London.

References

[1] J.T. Nelson, Recent developments in ground-borne noise and vibration control, *Journal of Sound and Vibration* 193 (1996) 367–376.
[2] C.J.C. Jones, J.R. Block, Prediction of ground vibration from freight train, *Journal of Sound and Vibration* 193 (1996) 205–213.
[3] X. Sheng, C.J.C. Jones, M. Petyt, Ground vibration generated by a harmonic load acting on a railway track, *Journal of Sound and Vibration* 225 (1999) 3–28.
[4] EN ISO 10846-2, Acoustics and vibration—laboratory measurement of vibro-acoustic transfer properties of resilient elements—Part 2: dynamic stiffness of elastic supports for translatory motion—direct method, August 2000.
[5] D.V. Jones, M. Petyt, Ground vibration in the vicinity of a strip load: a two-dimensional half-space model, *Journal of Sound and Vibration* 147 (1991) 155–166.